Low-dose carbon monoxide therapy is neuroprotective in rodent models of Parkinson's disease

Rose KN[1,2], Zorlu M[1], Xue X[1], Cai W[1], Lin S[1], Schwarzschild MA[1,2], Chen X[1,2], Gomperts SN[1,2]

1. Massachusetts General Hospital Institute for Neurodegenerative Diseases, Department of Neurology, Boston Ma, 02129
2. Harvard Medical School, Boston MA, 02115

ABSTRACT

Carbon monoxide (CO) has emerged as a potential neuroprotective agent that could underlie the reduced risk of Parkinson's disease (PD) among smokers. Here, we evaluated the neuroprotective potential of low dose CO treatment in PD models. In an AAV-alpha-synuclein (aSyn) model, rats underwent right nigral injection of AAV1/2- aSynA53T and left injection of empty AAV and were treated with oral CO drug product (HBI-002 10ml/kg, daily by gavage) or vehicle. In a short-term MPTP model (40mg/kg, i.p.), mice were treated with inhaled CO (iCO) (250ppm) or air. HPLC measurement of striatal dopamine, immunohistochemistry, stereological cell counting, and biochemical analyses were conducted blinded to treatment condition. Administration of HBI-002 in the aSyn model reduced ipsilateral loss of both striatal dopamine and tyrosine hydroxylase (TH)-positive neurons in the substantia nigra and reduced aSyn aggregates and S129 phosphorylation. In MPTP-exposed mice, low dose iCO reduced loss of dopamine and TH+ neurons. In saline-treated mice, iCO had no effect on striatal dopamine levels or TH+ cell counts. CO has been shown to activate PD-relevant cytoprotective cascades. Indeed,

HBI-002 increased both heme oxygenase-1 (HO-1) and HIF-1alpha. HBI-002 also increased Cathepsin D and Polo-like kinase 2, proteins that contribute to aSyn degradation. In human brain samples, HO-1 decorated Lewy bodies (LB), but HO-1 expression was greater in neurons without LB than neurons with LB pathology. These results demonstrating reduced dopamine cell death and aSyn pathology and engagement of PD-relevant molecular cascades advance low dose CO as a potential neuroprotective strategy for PD.

INTRODUCTION

Parkinson's disease (PD) is the second most common neurodegenerative disease, affecting an estimated 10 million individuals worldwide, yet has no proven disease modifying therapy. Pathologically, the disease is characterized by the spread of α-synuclein rich aggregates (i.e., Lewy bodies) and the degeneration of dopaminergic neurons in the substantia nigra pars compacta (SNpc). Extensive research into the epidemiology of PD has identified smoking tobacco as the environmental factor associated with the most reproducible reduction in PD risk(1, 2). This observation has prompted investigation into the therapeutic potential of tobacco smoke constituents, with nicotine the most well studied. Despite supportive pre-clinical data, however, clinical trials of nicotine have failed to demonstrate benefit on PD symptoms or progression(3, 4). Thus, other tobacco smoke constituents require evaluation. One plausible – if paradoxical – candidate that has yet to be investigated in PD is carbon monoxide (CO). The concentration of hemoglobin-bound CO (CO-Hb) is significantly higher in the blood of smokers than non-smokers, at levels of CO that activate cytoprotective cascades involving Nrf2 and HIF-1α and reduce neuroinflammation(5–10). These levels do not appear to be associated with CO toxicity(11, 12). *In vitro,* low-dose CO also increases the transcription of Nurr-1, a transcription

factor critical to the survival and maintenance of dopaminergic neurons(13, 14). In addition, over-expression of Nrf2-regulated heme oxygenase-1 (HO-1), a cytoprotective stress-induced enzyme that produces endogenous CO, has been found to protect dopamine cells from neurotoxicity in an animal model of PD(15). Given the potential for CO to underlie the inverse risk of smoking in PD via well-described cytoprotective cascades, we hypothesized that low-dose CO would confer protection in rodent models of PD.

RESULTS

To investigate the neuroprotective potential of CO we employed a genetic model of PD in which an AAV1/2 expression system drives the overexpression of mutant A53T human alpha-synuclein in the SNpc of rats, which results in loss of ipsilateral dopaminergic neurons after 21 days(16). Injection of empty AAV1/2 into the contralateral SNpc provided a vector-matched, within-animal control. Five days after injection, rats received either an oral CO drug product (HBI-002, Hillhurst Biopharmaceuticals) or HBI-002 vehicle daily by gavage for a total of 16 days. Administration of HBI-002 carrying CO reduced ipsilateral loss of both striatal dopamine (Figure 1a) and TH-positive neurons in the SNpc (Figure 1b,d) when compared to rats treated with HBI-002 vehicle. To determine if these effects were due to neuroprotection or to a change in TH expression, we stained for the neuronal marker NeuN. Compared to vehicle-treated animals, CO-treated animals had more NeuN-positive neurons in the ipsilateral SNpc (Figure 1c,e). Together, these results show that low-dose CO treatment increases survival of dopamine neurons in a progressive alpha-synuclein model of PD.

As aggregated alpha-synuclein is the principal pathological feature of PD, we next investigated the effect of low-dose CO on alpha-synuclein protein expression and accumulation in the soma. In serial sections of the SNpc stained for alpha-synuclein, CO treatment reduced the total alpha-synuclein (Figure 2 a,b). Because widespread phosphorylation of serine 129 (pSer129) is a pathological feature of PD-associated alpha-synuclein A53T toxicity(17), we next sought to evaluate pSer129-alpha-synuclein. Interestingly, low-dose CO treatment significantly reduced the amount of pSer129 staining (Figure 2 c,d). To further substantiate these findings, another group of rats underwent identical virus and low-dose CO treatments. Tissue blocks containing the SN were harvested, and immunoblotting revealed that CO treatment did not alter alpha-synuclein monomer expression (Figure 2 e,f) but did reduce pSer129-alpha-synuclein (Figure 2 e,g).

To identify potential mediators of low-dose CO's effects on phosphorylated and aggregated alpha-synuclein, we first evaluated the possibility that CO enhanced autophagy. Markers of autophagy including LC3bI/II ratio, p62, Rab4, and Vsp35 were largely unchanged (Figure 3 a,b). We therefore considered the possibility that CO enhanced alpha-synuclein degradation by enhancing lysosome activity. We observed no effect of CO treatment on the lysosome marker LAMP1 (Figure 3 a,b). In contrast, the expression of Cathepsin D, an aspartyl protease found in the lysosome, was markedly increased in ventral midbrains from rats treated with low-dose CO (Figure 3 a,b). As cathepsin D is one of the main proteases responsible for alpha-synuclein degradation and its upregulation has been shown to be neuroprotective(18–22), we sought to evaluate the effect of CO-induced increases of cathepsin D on its activity. In differentiated SH-SY5Y human neuroblastoma cells, CO treatment (200 ppm) significantly increased cathepsin D

activity (Figure 3 c,d). Additionally, the kinase Plk2 which phosphorylates alpha-synuclein at serine129(23) and has recently been demonstrated to facilitate the targeted degradation of alpha-synuclein(24, 25) was also upregulated with CO treatment (Figure 3 a,b). These data support the possibility that CO-induced increases in cathepsin D and Plk2 may underlie CO's ability to reduce the accumulation of alpha-synuclein and may contribute to its cytoprotective effects.

As PD is a complex disorder with many cellular cascades implicated in its pathogenesis and progression, it is advantageous to employ a variety of PD models to recapitulate distinct aspects of the disease. To build upon the data from our genetic rat model, we chose to use systemic administration of 1-methyl-4-phenyl-1,2,3,6-tetrahydropyridine (MPTP), which leads to rapid, reproducible, and specific lesioning of the nigrostriatal system(26) and recapitulates many features of PD including oxidative stress, mitochondrial disruption, ubiquitin-proteasome disruptions, and inflammation(27). To evaluate the efficacy of CO in this model, Male C57BL/6 mice received a single intraperitoneal dose of 40 mg/kg MPTP. One hour after MPTP administration, mice were treated with 225 ppm CO gas in room air or with ambient air for one hour. Five days following MPTP injection, mice were sacrificed for analysis. CO gas was employed for these experiments instead of HBI-002 as the pharmacokinetics of oral HBI-002 are less favorable in mice. In rats, a 10 ml/kg dose of HBI-002 elicits an increase in CO-Hb from 7.6 to 8.9% whereas in mice, the same dose increases CO-Hb from 2.6 to 3.1% (figure 4 a.) Treatment with CO gas, which resulted in 19.4 to 23.3% CO-Hb (figure 4a), attenuated MPTP-induced loss of striatal dopamine content (Figure 4 b), and stereology of the substantia nigra revealed reduced loss of tyrosine hydroxylase (TH)-positive neurons after CO treatment compared to mice exposed to air (Figure 4 c,d). To evaluate whether CO affected striatal

dopamine or nigral cell numbers, a second set of mice injected with saline underwent identical treatment with either CO or air. CO treatment had no effect on either striatal dopamine content or the number of TH-positive neurons (Figure 4 e,f). Together, these findings demonstrate that CO ameliorates MPTP toxicity in the nigrostriatal dopamine system.

As CO is a pleiotropic molecule that has been implicated in cytoprotective cascades(28), we set out to investigate its effects on another potential mediator of CO-associated neuroprotection, the cytoprotective protein HO-1(15). Studies in cellular and toxin models of PD have demonstrated an increase in HO-1 to be protective, and its overexpression has been associated with a reduction in alpha-synuclein aggregation(29–31). Furthermore, several studies have reported that CO exposure increases HO-1 expression(32–34). In line with these findings, we found that ventral midbrain HO-1 protein levels were significantly increased in rats treated with low-dose CO via HBI-002 compared to vehicle (Figure 5a). To dissect the mechanism by which CO could upregulate HO-1 expression, we first explored Nrf2-mediated transactivation of HMOX1(35). However, neither ventral midbrain Nrf2 nuclear translocation nor its activity was affected by treatment with low-dose CO (Figure 5 b-d). We therefore considered the possibility of CO-induced, HIF-1alpha mediated transactivation of HMOX1(36). Indeed, ventral midbrains from rats treated with low-dose CO had significantly increased nuclear HIF-1alpha expression compared to those treated with vehicle (Figure 2 b,e), suggesting that CO-induced HIF-1alpha nuclear translocation is responsible for the increased expression of HO-1.

To determine whether HO-1 expression is altered in human PD brain tissue, we evaluated HO-1 expression in anterior cingulate cortex samples from PD patients harboring neuropathologically

proven Lewy body disease, Alzheimer's disease (AD), or age matched normal controls. Overall, HO-1 expression was comparable across PD, AD, and control tissue (Figure 6a,b). These findings contrast with the previously reported increase in HO-1 expression in PD individuals in the substantia nigra(37) and in saliva(38). However, when we co-stained for the Lewy body marker pSer129-alpha-synuclein and HO-1, we observed a close association of HO-1 puncta surrounding Lewy bodies (Figure 6c). Thus, the association of HO-1 with Lewy bodies is not unique to PD dopamine cells(39). Furthermore, we observed that neurons harboring Lewy bodies had significantly lower expression of HO-1 when compared to adjacent neurons lacking Lewy bodies (Figure 6d,e). Together with the effects of low dose CO on reducing TH+ cell loss, on reducing aggregated and phosphorylated species of alpha-synuclein, and on increasing HO-1 expression, these neuropathological observations in human PD brain tissue suggest that neuronal HO-1 expression in PD may reflect a potentially protective response to PD-associated neuronal injury.

DISCUSSION

In this study, we demonstrate in genetic and toxin models of PD that treatment with low-dose CO preserves SNpc dopamine neurons along with striatal dopamine. Further, we show that CO treatment reduces alpha-synuclein pathology, the hallmark of PD. Low dose CO, as defined by levels associated with minimal toxicity, has recently been demonstrated to confer protection in numerous diseases, including traumatic brain injury, stroke(6, 7), sickle cell disease(40), and colitis(41). The present results thus extend CO's therapeutic potential to PD, and, potentially, to other neurodegenerative diseases of alpha-synuclein.

Consistent with prior reports implicating failure of lysosomal activity and cytoprotective cascades in PD(42, 43), CO's neuroprotective effects were associated with upregulation of Cathepsin D, Plk2, HO-1 and HIF-1alpha. CO's engagement of multiple PD-relevant mechanisms is consistent with the pleiotropic activity of CO, which binds with high affinity to heme containing proteins in the body and the brain(28). In addition to increasing lysosomal clearance of alpha-synuclein, Cathepsin D also generates Saposin C, a cofactor required for glucocerebrosidase function(44). Further research is required to determine the effects of CO-induced Cathepsin D on glucocerebrosidase activity.

As overexpression of HO-1 is protective in PD models(15, 29, 45), polymorphisms in HMOX1 have been associated with PD(46), and increased HO-1 levels have been reported in saliva samples in early PD(47), CO's induction of HO-1 is likely also disease-relevant. Building on the prior observation in PD brain tissue that HO-1 can be observed in Lewy body-laden dopamine cells, we found that HO-1 could be identified in Lewy body-containing neurons in the anterior cingulate cortex as well, another brain region affected early in PD. Even so, HO-1 expression was lower in neurons harboring Lewy bodies than in neurons lacking them. This observation raises the possibility that neuronal HO-1 upregulation may reflect a potentially protective, compensatory response to PD-associated injury. Further experiments will be required to test this hypothesis.

Together with the well-established reduced risk of PD among smokers(1, 2), the neuroprotective effects of low dose CO demonstrated in both an alpha-synuclein genetic model and an MPTP toxin model of PD, the engagement of PD-relevant cascades, and the findings in human brain

tissue increase the translational potential of low dose CO for PD. Further research is required to define the minimum effective dose and maximum tolerated dose of HBI-002 in animal models to guide translation to humans. In addition, it will be useful to determine whether treatment with low dose CO in humans increases levels of HO-1, Hif1alpha, and/or Cathepsin D in biofluids such as CSF or blood that can be used as biomarkers of target engagement.

Contrary to its high-risk profile at levels above 30% CO-Hb(48), CO has been found to be safe at levels up to 13.9% CO-Hb in 22 completed phase I and II clinical trials to date(49) (clinicaltrials.gov) including an ongoing evaluation of HBI-002 in healthy human volunteers (NCT03926819). As a gaseous formulation of CO would bring therapeutic complexity, including imprecise dosing and the risk of inadvertently over-dosing or dosing others, several non-gaseous formulations of CO have been developed for therapeutic use, including oral, IV, and rectally administered forms. An oral formulation that achieves safe and reliable dosing of CO is likely to have advantages for chronic use and has been used successfully in other pre-clinical animal models(50).

In the context of the epidemiologic foundation that has identified smoking tobacco as a large inverse risk factor for PD(1, 2), these results support the potential of low-dose CO to modify disease progression in PD. Given low-dose CO's favorable safety and pharmacokinetic profile, the present results demonstrating neuroprotection in PD models support further investigation of oral dosing of CO as a promising therapeutic candidate for PD.

MATERIALS AND METHODS

Study Design

The overall goal of this work was to evaluate the therapeutic potential of low dose CO in models of PD. For this purpose, we studied an oral liquid formulation of CO currently under development, HBI-002 (Hillhurst Biopharmaceuticals) and CO gas. We studied the efficacy of HBI-002 (oral gavage, 10 ml/kg) compared to HBI-002 vehicle in the AAV-aSynA53T rat model of PD (n = 13 per group). We studied the efficacy of CO gas (inhaled, 200 ppm) compared to air in the short term MPTP model of PD (n = 40 per group). Investigators were blinded to the HBI-002 versus HBI-002 vehicle intervention and were blinded for all analyses. Injection location was verified in every animal by visual inspection of the wound tract and alpha synuclein expression in target regions. Two animals were removed from the analysis because the stereotactic injection missed the substantia nigra. Another animal was excluded from dopamine analysis as dopamine levels were well above 100% of control, possibly due to improper dissection of the striatum. This animal was identified as an outlier by the ROUT method. Each study was replicated 2 times. The data provided are biological replicates of a single study.

Animals

Six-month-old male C57BL/6 mice were purchased from The Jackson Laboratory (Bar Harbor, ME) and female Sprague Dawley rats ranging from 220-240 g were purchased from Charles River (Wilmington, MA). All animals were housed in the Center for Comparative Medicine at Massachusetts General Hospital's Institute for Neurodegenerative diseases with a 12hr light/dark cycle and access to food and water *ad libitum*. All experiments were approved by Massachusetts General Hospital's institutional animal care and use committee (protocol # 2015N00014, 2019N00168).

Overexpression of human A53T alpha-synuclein in the SNpc of rats

Rats were anesthetized with isoflurane/oxygen and underwent bilateral stereotactic surgery. Each animal received 2 μL of a $5x10^{12}$ GC/mL viral titer injected into the nigra at the following coordinates: AP: -5.2, ML: +/- 2.0, DV: -7.8. The left nigra received AAV1/2-CMV-empty vector-WPRE-BGH-polyA; the right nigra received AAV1/2-CMV-human-A53T-alpha-sunuclein-WPRE-BGH-polyA. Viruses were purchased from Vigene Biosciences (Rockville, MD). Animals were allowed to recover for 5 days before interventions began.

Oral carbon monoxide treatment

A liquid carbon monoxide drug product, referred to as HBI-002, was provided by Hillhurst Biopharmaceuticals, Inc. (Montrose, CA). HBI-002 or vehicle (HBI-002 formulation without CO) was given to animals via oral gavage (14 GA needle) at a dose of 10 mL/kg/day. Both HBI-002 and vehicle were stored and administered at 4°C.

HBI-002 pharmacokinetics

Animals were deeply anesthetized with an overdose of ketamine/xylazine followed by cardiac puncture into the right ventricle. Blood was collected using a 3 mL heparin coated line-draw syringe and a 23 Ga. needle. Blood samples were then immediately analyzed for CO-Hb% by oximetry using an Avoximeter 4000 (Instrumentation Laboratory, Bedford, MA).

MPTP administration in mice and gaseous CO administration

Mice were given an i.p. injection of 40mg/kg MPTP or saline. One hour following injections, mice were treated with CO gas (250ppm, 1 L/min) or air (1 L/min) for one hour by placing animals in a chamber with a constant flow of gas. Five days after treatment, animals were sacrificed via cervical dislocation and their brains harvested for further processing.

Quantification of dopamine by HPLC-ECD

Animals were deeply anesthetized with ketamine and xylazine followed by rapid decapitation and brain removal. The striatum from each hemisphere was segregated, dissected on ice, and frozen on dry ice. Pieces of frozen striatum were weighed and homogenized in 0.1 mM EDTA, 1 μM 3,4 dihydroxybenzlamine hydrobromide (DHBA, internal standard), and 50 mM phosphoric acid in a 1:20 ratio (weight:volume). The resulting homogenate was centrifuged at 14,000 x g to pellet cell debris and precipitated protein. The supernatant was then filtered through Costar SpinX 0.22-micron spin filter cartridges (Sigma-Aldrich). After filtering, 5 μL of supernatant was injected onto a Microsorb-MV column (C18, 150 mm x 5.6 mm, 5 micron) using an Ultimate 3000 UHPLC system (Thermo Fisher). Separation was achieved with a 17-minute isocratic method at a flow rate of 0.6 mL/min, and a mobile phase consisting of 75 mM sodium phosphate monobasic, 1.75 mM sodium-1-octanesulfonate, 100 μL/L triethylamine, 25 μM EDTA, and 10% acetonitrile. Detection was carried out with an Ultimate 3000 ECD-3000RS (Thermo Fisher) with a screening electrode set to -150 mV and a detection electrode set to 250 mV. DHBA was used as an internal standard and dopamine concentration was calculated from a standard curve. Analyses were blinded to experimental conditions.

Immunohistochemistry

Blocks of tissue containing the SNpc were drop-fixed in 4% paraformaldehyde for three days. After that time, brains were sectioned at 40 μm on a vibratome (Leica, Buffalo Grove, IL). Sections were collected in a 1 in 6 series and stored in PBS at 4°C. For each antigen, a single series of sections were stained from each animal. Free-floating sections were incubated in 3% hydrogen peroxide for 15 minutes to block endogenous peroxidase. Next, sections were blocked and permeabilized in PBS with 2.5% bovine serum albumin (BSA), 10% normal goat serum (NGS), and 0.3% Triton X-100 for 30 minutes. Sections were then transferred to wells containing the corresponding primary antibody diluted in PBS with 2.5% BSA and 10% NGS. Primary antibodies used were tyrosine hydroxylase (Abcam cat# ab112, 1:1000), NeuN (BioLegend cat# 834501, 1:2000), alpha-synuclein (ThermoFisher cat# 32-8100, 1:1000), p-ser129 alpha-synuclein (Biolegend cat# 825702, 1:1000). Sections were allowed to incubate overnight at 4°C. After several washes in PBS, antigens were visualized using an avidin-biotin detection system (ABC elite kit, Vector, Burlingame, CA) with ImmPact VIP and DAB substrates (Vector, Burlingame, CA) following the manufacturer's instructions. Sections were mounted, dehydrated in graded ethanol, cleared in xylene, and cover slipped with permanent mounting media (VectaMount, Vector, Burlingame, CA). In instances where sections were counterstained, hematoxylin QS (Vector, Burlingame, CA) was used per the manufacturer's instructions.

Human tissue

Brain tissue samples from 4 donors with PD, 4 donors with AD, and 3 donors without neurodegenerative disease were selected from the Massachusetts Alzheimer's Disease Research Center (MADRC) Neuropathology Core, which obtained written informed consent from next-of-

kin for brain donation. Brains donated to the MADRC have undergone full brain autopsy and neuropathological confirmation of diagnosis, with comprehensive assessment of primary and co-pathologies. Brains from PD patients had high Lewy body pathology (Lewy body disease Braak stage 5-6) and met criteria for Lewy body disease.(51) Brains from AD patients had high amyloid and tau pathology and no Lewy body disease pathology (Thal stage 4-5, Braak stage VI, LBD Braak stage 0) and met criteria for Alzheimer's disease according to NIA-AA guidelines.(52) Tissue from the anterior cingulate region was used.

For staining human tissue, formalin-fixed, paraffin embedded sections were cleared in xylene and brought to TBS through graded ethanol and water. Antigen retrieval was performed by boiling sections in 10mM citric acid (pH=6) for 30 minutes followed by a 20-minute cooldown. Lipofuscin was blocked using TrueBlack (Biotium, Freemont, CA) following the manufacturer's instructions. Sections were then blocked with 10% BSA and 2.5% NGS. The primary antibodies used were p-ser129 alpha-synuclein (FujiFilm cat# 015-25191, 1:1000) and HO-1 (Cell Signaling cat# 26416, 1:200). Sections were allowed to incubate overnight at 4°C. Following several washes in TBS, sections were incubated in anti-mouse Alexa Fluor 555 and anti-rabbit Alexa Fluor 488 (Thermo Fisher cat# A-21422 and A-11008, respectively). After several washed in TBS, sections were incubated with anti-HuD directly conjugated to Alex Fluor 647 (Santa Cruz cat# sc-28299, 1:50) for 1 hour at room temperature, followed by several washed in TBS, cover slipping with anti-fade mounting media, and imaged. ImageJ was used for staining intensity quantification. Analyses were blinded to experimental conditions when possible.

Stereology

Sections labeled with TH, NeuN, and alpha-synuclein underwent counting using the optical fractionator principles with CAST stereology software (Olympus, Tokyo, Japan). Experimenters were blinded to experimental conditions. Counting was limited to the substantia nigra and was done with a 20X objective with a meander sampling of 100% to count the entire region. A total of six sections spanning the SNpc were counted per animal.

ELISA

HO-1 was quantified using an ELISA (Enzo Life Sciences, Farmingdale, NY) specific to rat HO-1. HO-1 concentration was determined using a standard curve, and values are reported as ng HO-1/mg protein. Analyses were blinded to experimental conditions.

Protein Extraction

Using a matrix, 3 mm blocks of brain tissue containing the SNpc were dissected. Then, a 3 mm biopsy punch was used to dissect the tissue containing the SNpc. The tissue punches were then homogenized in TBS with a protease and phosphatase inhibitor cocktail (Sigma Alrdich, St Louis, MO). The resulting homogenate was cleared by centrifugation at 100,000 x g for 1 hour at 4°C. For nuclear protein extractions, fresh tissue was homogenized in Dounce homogenizers using NE-PER (Thermo Fisher cat#78833) fowling the manufacturers instructions.

Immunoblotting

Samples were diluted in 2x Lamelli buffer and heated at 70°C for 10 minutes. Samples were then loaded on a 10-20% polyacrylamide gel and electrophoresis was carried out at 225 V until the dye front reached the bottom of the gel. Then, proteins were transferred to PVDF membranes,

washed in distilled water, and dried overnight at 4°C. After reactivation of the PVDF membrane in methanol, total protein per lane was quantified using Revert 700 total protein stain and an Odyssey CLx imaging system (Licor, Lincoln, NE) on the 700 nm channel per the manufacturer's instructions. Membranes were then blocked in 5% dry non-fat milk powder in TBS for 1 hour at room temperature followed by overnight incubation at 4°C in primary antibody diluted in 5% dry non-fat milk powder in TBS-T. Primary antibodies used were: alpha-synuclein (ThermoFisher cat# 32-8100, 1:1000), p-ser129 alpha-synuclein (FujiFilm cat# 015-25191, 1:1000), LC3b (Novus cat# NB600-1384, 1:1000), p62 (Abcam cat# ab109012, 1:10,000), RAB4 (Abcam cat# ab109009, 1:1000), VSP35 (Invitrogen cat# PA5-21898, 1:1000), Lamp-1 (Invitrogen cat# MA5-29384, 1:500) Ctsd (Cell Signaling cat# 69854, 1:1000), Plk2 (Novus cat# NBP2-15078, 1:500), Nrf2 (Novus NBP1-32822, 1:1000), and HIF-1α (Novus cat# NB100-449, 1:1000). After several washes in TBS-T, membranes were incubated in a 1:30:000 dilution of IRDye 800 donkey anti-rabbit or anti-mouse (Licor, Lincoln, NE) in 5% dry non-fat milk powder and 0.02% SDS in TBS-T for 1 hour at room temperature. For p-ser129 alpha-synuclein, 50mM NaF was added to all milk-based buffers. After several washes in TBS-T followed by a final wash in TBS, blots were imaged with an Odyssey CLx imaging system on the 800 nm channel. Fluorescent intensity of bands was determined using Image Studio (Licor, Lincoln, NE) and bands were normalized to total protein loaded in individual lanes. Three technical replicates were used for quantification purposes. Analyses were blinded to experimental conditions.

Cell culture

Human neuroblastoma SH-SY5Y cells were purchased from American Type Culture Collection (ATCC, VA, USA) and maintained in high glucose DMEM supplemented with 10% FBS and 1% P/S. Cells were kept in a 5% CO_2 incubator set at 37°C.

Cell culture carbon monoxide exposure

For treatment with CO, cells were transferred to a portable incubator (5% CO_2 ,37°C) set inside a fume hood. Compressed CO (200 ppm) was plumbed directly into the incubator. For the 5 hours of treatment, a constant flow of 5L/min at 1 psi CO was applied to the incubator. After the treatment, cells were returned to their home incubator.

Nrf2 activity assay

Nrf2 activity was quantified using nuclear extracts and a TransAm NRF2 activity kit from Active Motif (cat# 50296) following the manufacturers included instructions.

Cathepsin D activity assay

SH-SY5Y cells were grown on chamber slides to confluency. Cells were then treated with CO for five hours and returned to their home incubator. Twenty-four hours after starting CO treatment, active cathepsin D was stained for using the sir-Lysosome probe per the manufacturer instructions (Spirochrome, Rhein, Switzerland). Images were taken at 63X under oil immersion. Sir-lysosome fluorescence was measured by ImageJ and at least 15 cells were counted per condition.

Statistical analyses

Data are expressed as means ± SEM. Unpaired T-tests were used to analyze two groups. Analysis of variance (ANOVA) was used for multiple comparisons, with Tukey post-hoc P values for pairwise comparisons. $P < 0.05$ was considered significant. Analyses were performed with GraphPad Prism.

Data availability

The datasets generated and analyzed in the current study are available from the corresponding author on reasonable request.

REFERENCES

1. L. Fratiglioni, H.-X. Wang, Smoking and Parkinson's and Alzheimer's disease: review of the epidemiological studies. *Behav. Brain Res.* **113**, 117–120 (2000).

2. V. Gallo, *et al.*, Exploring causality of the association between smoking and Parkinson's disease. *Int. J. Epidemiol.* **48**, 912–925 (2019).

3. G. Villafane, *et al.*, High-dose transdermal nicotine in Parkinson's disease patients: a randomized, open-label, blinded-endpoint evaluation phase 2 study. *Eur. J. Neurol.* **25**, 120–127 (2018).

4. W. Oertel, *et al.*, The NIC-PD-study –A randomized, placebo- controlled, double-blind, multi-centre trial to assess the disease-modifying potential of transdermal nicotine in early Parkinson's disease in Germany and N. America. 1.

5. R. D. Stewart, The Effect of Carbon Monoxide on Humans. *Annu Rev Pharmacol* **15**, 409–423 (1975).

6. B. Wang, W. Cao, S. Biswal, S. Doré, Carbon Monoxide–Activated Nrf2 Pathway Leads to Protection Against Permanent Focal Cerebral Ischemia. *Stroke* **42**, 2605–2610 (2011).

7. Y. K. Choi, *et al.*, Dual effects of carbon monoxide on pericytes and neurogenesis in traumatic brain injury. *Nat. Med.* **22**, 1335–1341 (2016).

8. L. E. Otterbein, *et al.*, Carbon monoxide has anti-inflammatory effects involving the mitogen-activated protein kinase pathway. *Nat. Med.* **6**, 422–428 (2000).

9. B. Y. Chin, *et al.*, Hypoxia-inducible factor 1 stabilization by carbon monoxide results in cytoprotective preconditioning. *Proc. Natl. Acad. Sci.* **104**, 5109–5114 (2007).

10. M. Bilban, *et al.*, Carbon Monoxide Orchestrates a Protective Response through PPARγ. *Immunity* **24**, 601–610 (2006).

11. Carbon Monoxide | Toxicological Profile | ATSDR (May 15, 2023).

12. R. D. Stewart, *et al.*, Experimental human exposure to carbon monoxide. *Arch. Environ. Health* **21**, 154–164 (1970).

13. N. Dreyer-Andersen, *et al.*, Intermittent, low dose carbon monoxide exposure enhances survival and dopaminergic differentiation of human neural stem cells. *PLOS ONE* **13**, e0191207 (2018).

14. B. Kadkhodaei, *et al.*, Nurr1 Is Required for Maintenance of Maturing and Adult Midbrain Dopamine Neurons. *J. Neurosci.* **29**, 15923–15932 (2009).

15. S.-Y. Hung, *et al.*, Overexpression of Heme Oxygenase-1 Protects Dopaminergic Neurons against 1-Methyl-4-Phenylpyridinium-Induced Neurotoxicity. *Mol. Pharmacol.* **74**, 1564–1575 (2008).

16. J. B. Koprich, T. H. Johnston, M. G. Reyes, X. Sun, J. M. Brotchie, Expression of human A53T alpha-synuclein in the rat substantia nigra using a novel AAV1/2 vector produces a rapidly evolving pathology with protein aggregation, dystrophic neurite architecture and nigrostriatal degeneration with potential to model the pathology of Parkinson's disease. *Mol. Neurodegener.* **5**, 43 (2010).

17. H. Sato, *et al.*, Authentically Phosphorylated -Synuclein at Ser129 Accelerates Neurodegeneration in a Rat Model of Familial Parkinson's Disease. *J. Neurosci.* **31**, 16884–16894 (2011).

18. D. Sevlever, P. Jiang, S.-H. C. Yen, Cathepsin D is the main lysosomal enzyme involved in the degradation of alpha-synuclein and generation of its carboxy-terminally truncated species. *Biochemistry* **47**, 9678–9687 (2008).

19. E.-J. Bae, *et al.*, Haploinsufficiency of cathepsin D leads to lysosomal dysfunction and promotes cell-to-cell transmission of α-synuclein aggregates. *Cell Death Dis.* **6**, e1901–e1901 (2015).

20. S. Prieto Huarcaya, *et al.*, Recombinant pro-CTSD (cathepsin D) enhances SNCA/α-Synuclein degradation in α-Synucleinopathy models. *Autophagy* **18**, 1127–1151 (2022).

21. V. Cullen, *et al.*, Cathepsin D expression level affects alpha-synuclein processing, aggregation, and toxicity in vivo. *Mol. Brain* **2**, 5 (2009).

22. L. Qiao, *et al.*, Lysosomal enzyme cathepsin D protects against alpha-synuclein aggregation and toxicity. *Mol. Brain* **1**, 17 (2008).

23. K. J. Inglis, *et al.*, Polo-like Kinase 2 (PLK2) Phosphorylates α-Synuclein at Serine 129 in Central Nervous System. *J. Biol. Chem.* **284**, 2598–2602 (2009).

24. M. Dahmene, M. Bérard, A. Oueslati, Dissecting the Molecular Pathway Involved in PLK2 Kinase-mediated α-Synuclein-selective Autophagic Degradation. *J. Biol. Chem.* **292**, 3919–3928 (2017).

25. Polo-like kinase 2 regulates selective autophagic α-synuclein clearance and suppresses its toxicity in vivo https:/doi.org/10.1073/pnas.1309991110 (May 8, 2023).

26. V. Jackson-Lewis, S. Przedborski, Protocol for the MPTP mouse model of Parkinson's disease. *Nat. Protoc.* **2**, 141–151 (2007).

27. G. E. Meredith, D. J. Rademacher, MPTP Mouse Models of Parkinson's Disease: An Update. *J. Park. Dis.* **1**, 19–33 (2011).

28. Z. Yuan, L. K. De La Cruz, X. Yang, B. Wang, Carbon Monoxide Signaling: Examining Its Engagement with Various Molecular Targets in the Context of Binding Affinity, Concentration, and Biologic Response. *Pharmacol. Rev.* **74**, 823–873 (2022).

29. J. K. Youn, *et al.*, PEP-1-HO-1 prevents MPTP-induced degeneration of dopaminergic neurons in a Parkinson's disease mouse model. *BMB Rep.* **47**, 569–574 (2014).

30. W. Song, *et al.*, The Parkinson disease-associated A30P mutation stabilizes α-synuclein against proteasomal degradation triggered by heme oxygenase-1 over-expression in human neuroblastoma cells. *J. Neurochem.* **110**, 719–733 (2009).

31. Q. He, *et al.*, Role of α-synuclein aggregation and the nuclear factor E2-related factor 2/heme oxygenase-1 pathway in iron-induced neurotoxicity. *Int. J. Biochem. Cell Biol.* **45**, 1019–1030 (2013).

32. C.-C. Lin, C.-C. Yang, L.-D. Hsiao, S.-Y. Chen, C.-M. Yang, Heme Oxygenase-1 Induction by Carbon Monoxide Releasing Molecule-3 Suppresses Interleukin-1β-Mediated Neuroinflammation. *Front. Mol. Neurosci.* **10**, 387 (2017).

33. B. Wang, W. Cao, S. Biswal, S. Doré, Carbon monoxide-activated Nrf2 pathway leads to protection against permanent focal cerebral ischemia. *Stroke J. Cereb. Circ.* **42**, 2605–2610 (2011).

34. B. S. Zuckerbraun, *et al.*, Carbon Monoxide Protects against Liver Failure through Nitric Oxide–induced Heme Oxygenase 1. *J. Exp. Med.* **198**, 1707–1716 (2003).

35. J. F. Reichard, G. T. Motz, A. Puga, Heme oxygenase-1 induction by NRF2 requires inactivation of the transcriptional repressor BACH1. *Nucleic Acids Res.* **35**, 7074–7086 (2007).

36. P. J. Lee, *et al.*, Hypoxia-inducible Factor-1 Mediates Transcriptional Activation of the Heme Oxygenase-1 Gene in Response to Hypoxia. *J. Biol. Chem.* **272**, 5375–5381 (1997).

37. I. Lastres-Becker, *et al.*, α-Synuclein expression and Nrf2 deficiency cooperate to aggravate protein aggregation, neuronal death and inflammation in early-stage Parkinson's disease. *Hum. Mol. Genet.* **21**, 3173–3192 (2012).

38. J. M. Galindez, *et al.*, Salivary Heme Oxygenase-1: A Potential Biomarker for Central Neurodegeneration. *J. Cent. Nerv. Syst. Dis.* **13**, 11795735211029114 (2021).

39. H. M. Schipper, A. Liberman, E. G. Stopa, Neural Heme Oxygenase-1 Expression in Idiopathic Parkinson's Disease. *Exp. Neurol.* **150**, 60–68 (1998).

40. J. D. Belcher, *et al.*, Oral carbon monoxide therapy in murine sickle cell disease: Beneficial effects on vaso-occlusion, inflammation and anemia. *PloS One* **13**, e0205194 (2018).

41. T. Takagi, *et al.*, Carbon monoxide ameliorates murine T-cell-dependent colitis through the inhibition of Th17 differentiation. *Free Radic. Res.* **52**, 1328–1335 (2018).

42. O. A. Levy, C. Malagelada, L. A. Greene, Cell death pathways in Parkinson's disease: proximal triggers, distal effectors, and final steps. *Apoptosis* **14**, 478–500 (2009).

43. B. Dehay, *et al.*, Lysosomal impairment in Parkinson's disease: Lysosomal Impairment In PD. *Mov. Disord.* **28**, 725–732 (2013).

44. N. Tayebi, G. Lopez, J. Do, E. Sidransky, Pro-cathepsin D, Prosaposin, and Progranulin: Lysosomal Networks in Parkinsonism. *Trends Mol. Med.* **26**, 913–923 (2020).

45. N. Yamamoto, *et al.*, Elevation of heme oxygenase-1 by proteasome inhibition affords dopaminergic neuroprotection. *J. Neurosci. Res.* **88**, 1934–1942 (2010).

46. P. Ayuso, *et al.*, An association study between Heme oxygenase-1 genetic variants and Parkinson's disease. *Front. Cell. Neurosci.* **8** (2014).

47. W. Song, *et al.*, Evaluation of salivary heme oxygenase-1 as a potential biomarker of early Parkinson's disease. *Mov. Disord. Off. J. Mov. Disord. Soc.* **33**, 583–591 (2018).

48. M. L. Bleecker, Carbon monoxide intoxication. *Handb. Clin. Neurol.* **131**, 191–203 (2015).

49. E. Gomperts, *et al.*, The Role of Carbon Monoxide and Heme Oxygenase in the Prevention of Sickle Cell Disease Vaso-Occlusive Crises. *Am. J. Hematol.* **92**, 569–582 (2017).

50. J. D. Byrne, *et al.*, Delivery of therapeutic carbon monoxide by gas-entrapping materials. *Sci. Transl. Med.* **14**, eabl4135 (2022).

51. H. Braak, E. Ghebremedhin, U. Rüb, H. Bratzke, K. Del Tredici, Stages in the development of Parkinson's disease-related pathology. *Cell Tissue Res.* **318**, 121–134 (2004).

52. B. T. Hyman, *et al.*, National Institute on Aging-Alzheimer's Association guidelines for the neuropathologic assessment of Alzheimer's disease. *Alzheimers Dement. J. Alzheimers Assoc.* **8**, 1–13 (2012).

ACKNOWLEDGEMENTS

The authors thank Nitsan Goldstein (MGH, Department of Neurology) for research assistance.

Research reported in this publication was supported by grants from the Farmer Family Foundation Parkinson's Research Initiative (FFFPRI), the Michael J. Fox Foundation, and the NIH (R41 NS122576).

AUTHOR CONTRIBUTIONS

KNR contributed to the design, acquisition, analysis, and interpretation of data, as well as to the drafting of the manuscript.

MZ contributed to the design, to the acquisition, analysis, and interpretation of data, and to the review of the manuscript.

XX contributed to the acquisition, analysis, and interpretation of data, and to the review of the manuscript.

CW contributed to the acquisition, analysis, and interpretation of data, and to the review of the manuscript.

SL contributed to the design, to the acquisition, analysis, and interpretation of data, and to the review of the manuscript.

MAS contributed to interpretation of data and the review of the manuscript.

XC contributed to the design, analysis, interpretation of data, and the review of the manuscript.

SNG contributed to the conception, design, analysis, and interpretation of data, and to the drafting of the manuscript.

MATERIALS AND CORRESPONDENCE

Stephen Gomperts, MD, PhD

Massachusetts General Hospital Institute for Neurodegenerative Diseases

114 16th Street

Charlestown, MA 02129

FIGURES AND FIGURE LEGENDS

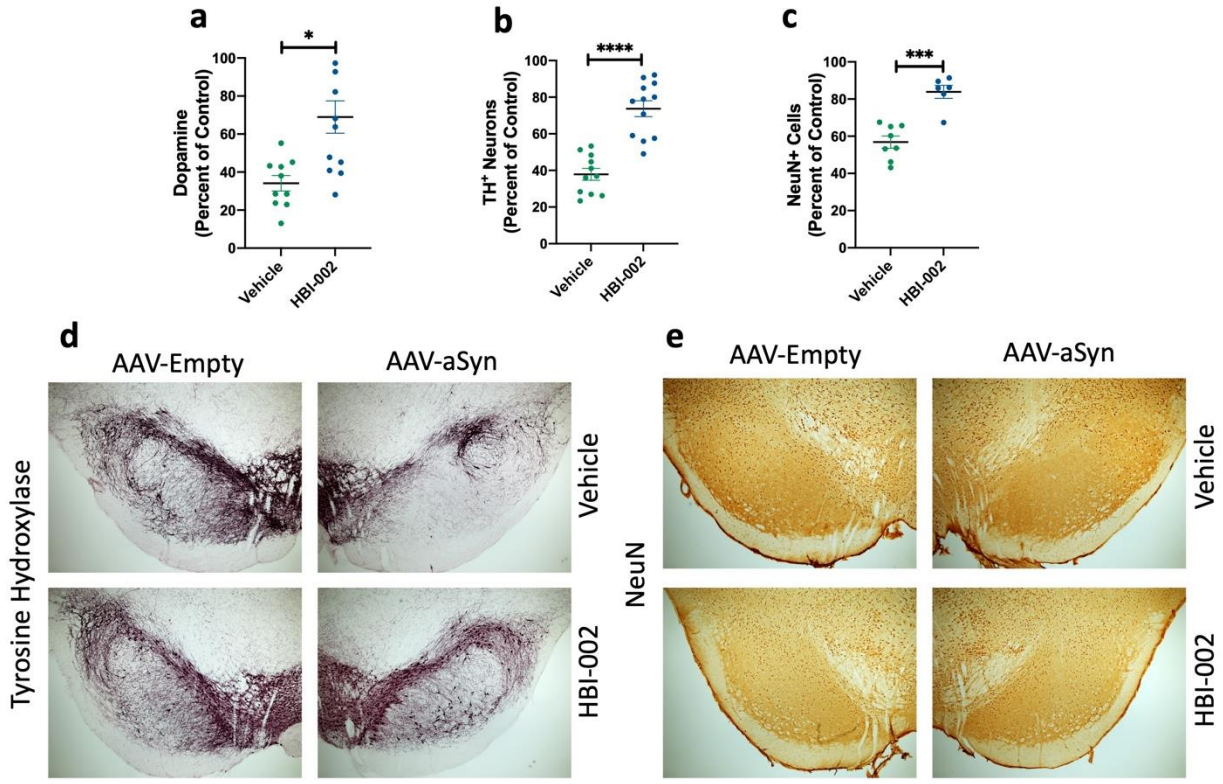

Figure 1. HBI-002, an oral formulation of CO, protects against human mutant A53T alpha-synuclein (aSyn) neurotoxicity. The left nigra received AAV1/2-CMV-empty vector-WPRE-BGH-polyA (Control); the right nigra received AAV1/2-CMV-human-A53T-alpha-sunuclein-WPRE-BGH-polyA. **(a)** Quantification of striatal dopamine by HPLC-ECD. P=0.0024, N=22. **(b)** Quantification of TH+ cells in the SN. P=0.0001, N=26. **(c)** Quantification of NeuN+ cells in the SN. P=0.001, N=15. **(d)** Representative photomicrographs of TH in the SN. **(e)** Representative photomicrographs of NeuN in the SN. Error bars represent the mean ± SEM.

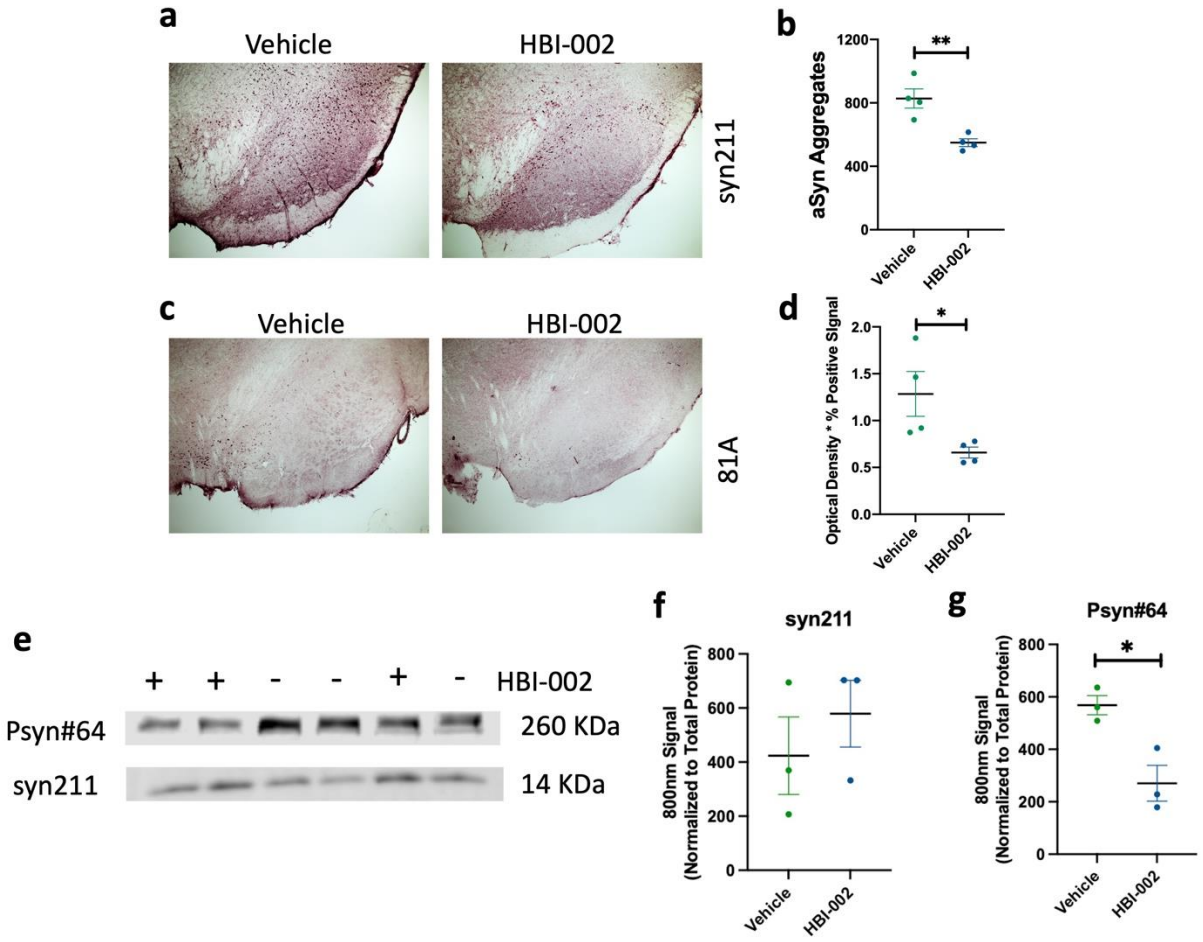

Figure 2 . HBI-002 modulates aSyn pathology in an AAV-A53T model of PD. **(a)** Representative photomicrographs of aSyn immunoreactivity in the SN using the c-terminal specific antibody syn211. **(b)** Quantification of aggregated aSyn in the SN, values represent actual counted aggregates. P=0.02, N=8. **(c)** Representative photomicrographs of aSyn immunoreactivity in the SN using the serine-129 phosphorylation specific antibody 81A. **(d)** Quantification of pSer129-aSyn in the SN P=0.0053, N=8. **(e)** Immunoblots of aggregated aSyn (260 KDa) and monomeric aSyn (14 KDa). **(f)** Quantification of aSyn monomers. P=0.69, N=6. **(g)** Quantification of aggregated pSer129-aSyn. P=0.0014, N=6. Error bars represent the mean ± SEM.

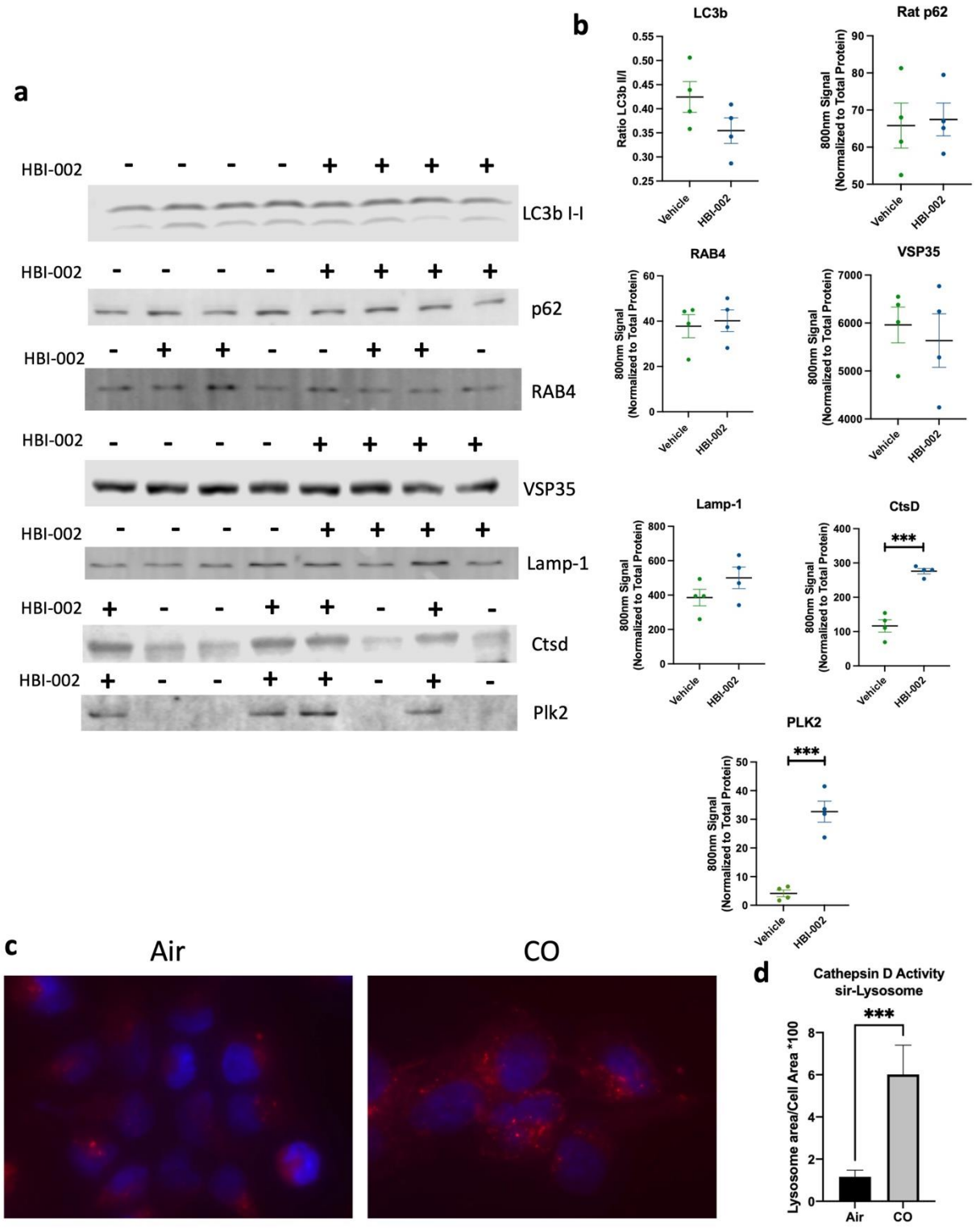

Figure 3. HBI-002 effects on autophagy, lysosomes and cathepsin D expression. ***(a)*** Immunoblots of autophagy and lysosomal activity markers. **(b)** Quantification of autophagy and lysosomal activity markers Ctsd (p=0.002 N=8) and Plk2 (p=0.006 N=8) all other markers p>0.05. **(c)** Representative photomicrographs of sir-lysosome staining in SH-SY5Y human neuroblastomas. **(d)** Quantification of sir-lysosome staining p=0.0002, N=38.

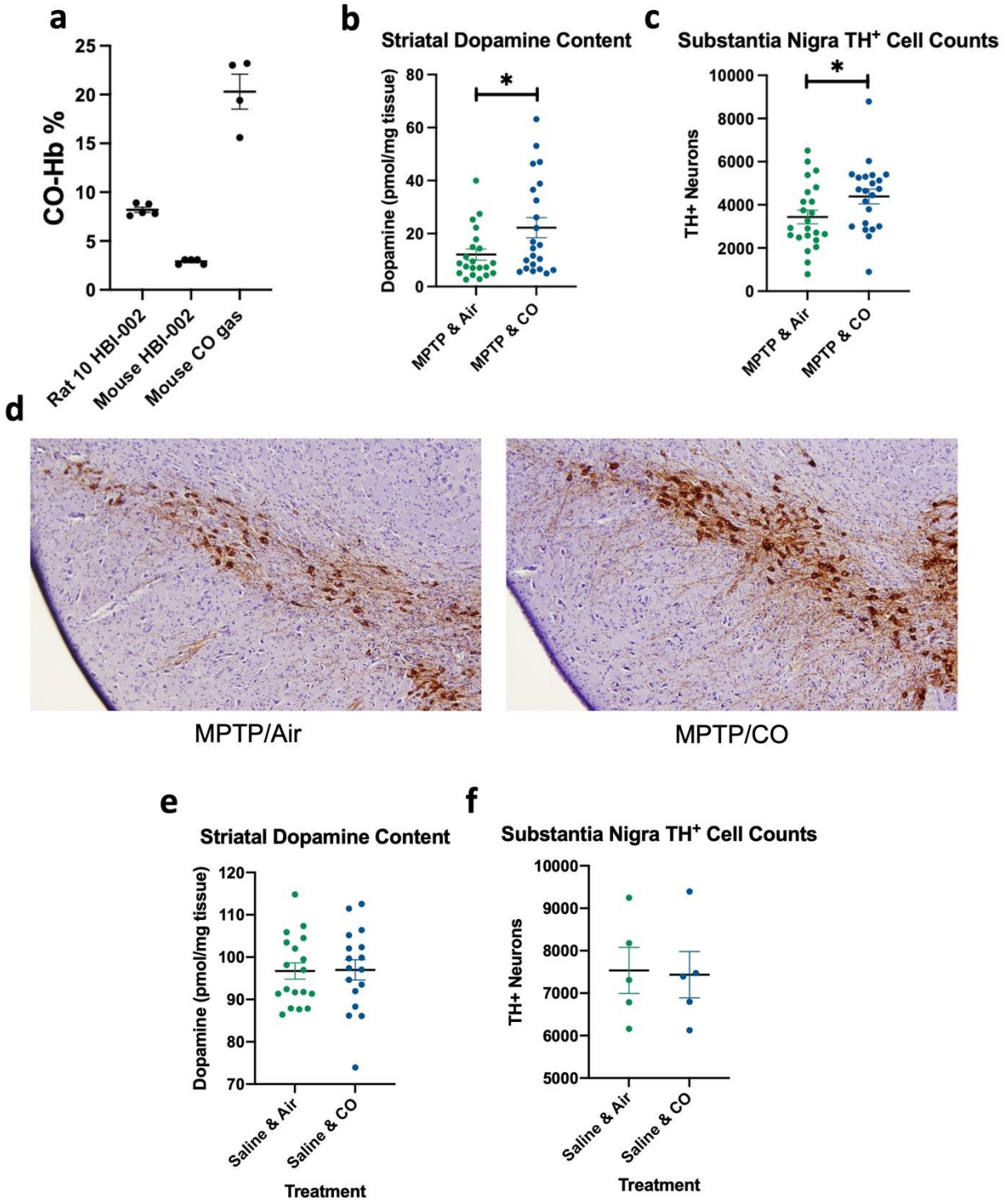

Figure 4. Carbon monoxide protects against MPTP induced neurotoxicity in the SN. **(a)** C_{max} of CO across different species and delivery methods of CO. **(b)** HPLC-ECD quantification of striatal dopamine content. N=79, P=0.03 **(c)** Quantification of TH-positive cells in the SNpc. N=79, P=0.04. **(d)** Representative photomicrographs of TH immunoreactivity in the SN, counterstained with hematoxylin QS. **(e)** HPLC-ECD quantification of striatal dopamine content in animals not given MPTP, P > 0.05. **(f)** Quantification of TH+ cells in the SNpc in mice not treated with MPTP, P > 0.05. Error bars represent the mean ± SEM.

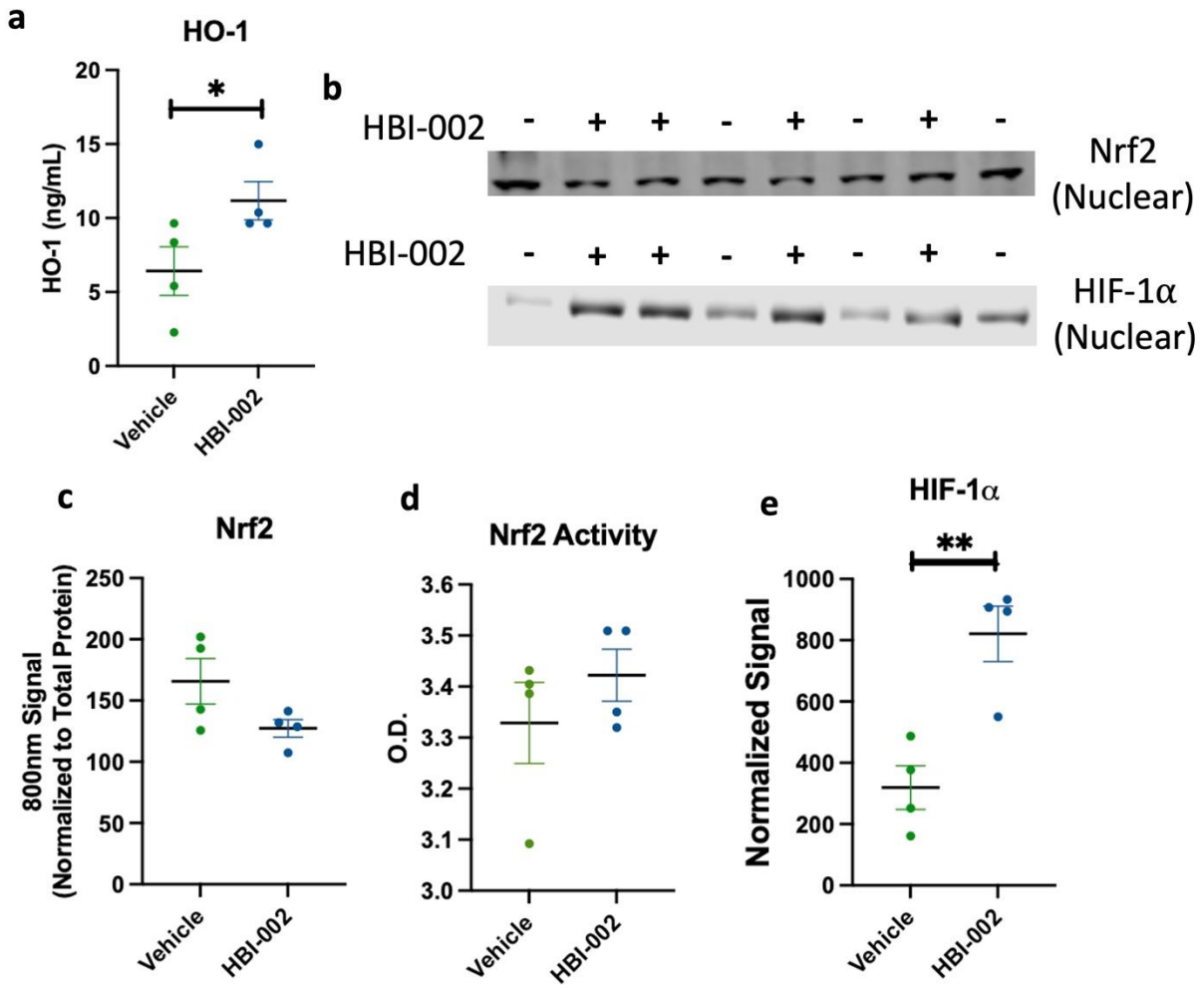

Figure 5. Carbon monoxide increases the expression of HO-1 in association with increased HIF-1α signaling. ***(a)*** *Quantification of HO-1 by ELISA P=0.0428 N=14.* ***(b)*** Immunoblots of nuclear Nrf2 and *HIF-1α.* ***(c)*** *Quantification of nuclear Nrf2 P>0.05.* ***(d)*** Quantification of nuclear Nrf2 activity P>0.05. **(e)** *Quantification of nuclear HIF-1α P=0.0048 N=8.* Error bars represent the mean ± SEM.

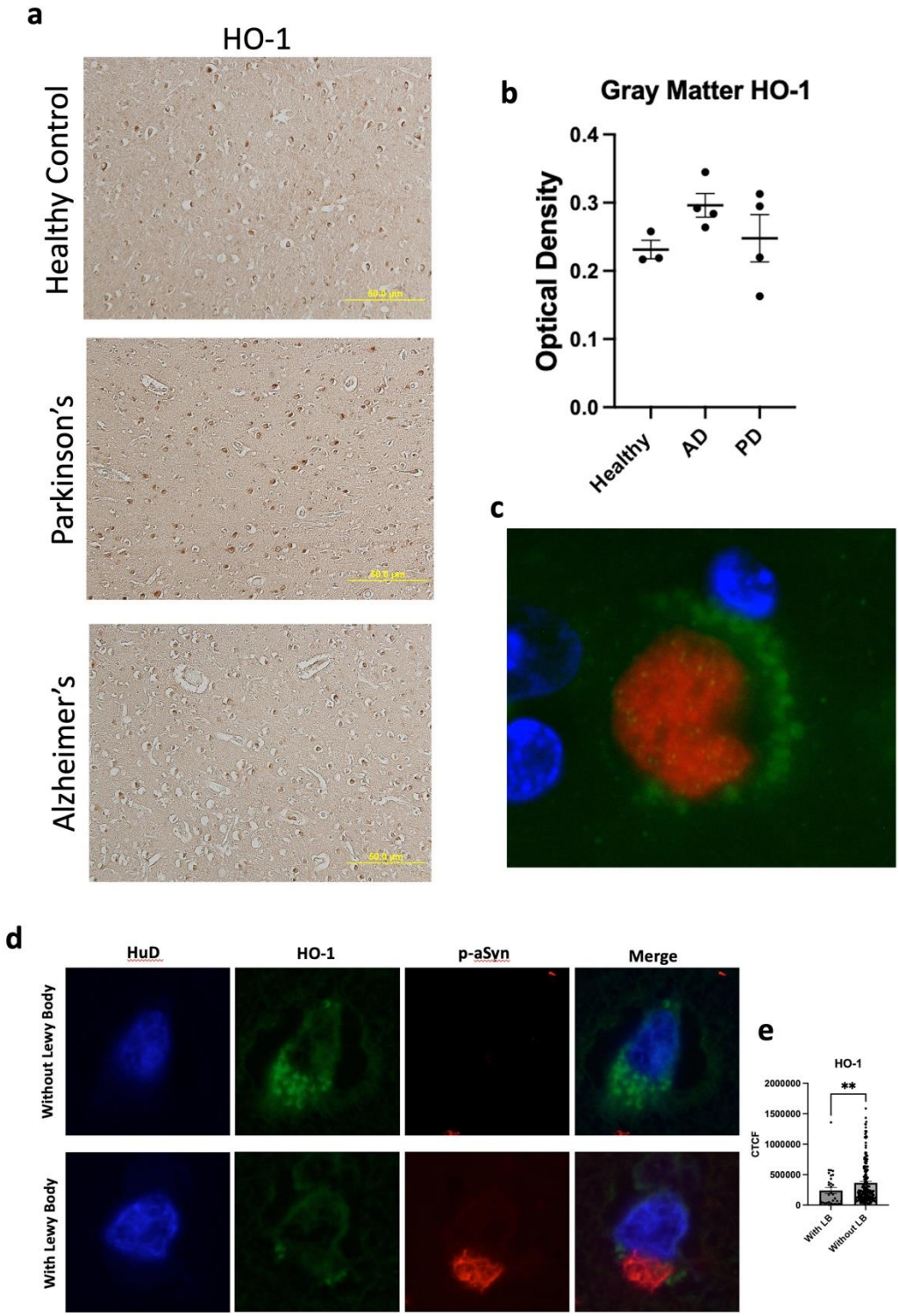

Figure 6. HO-1 is associated with cortical Lewy bodies. **(a)** Representative photomicrographs of HO-1 immunoreactivity in the anterior cingulate of healthy controls or patients who dies with AD or PD. **(b)** Quantification of HO-1 immunoreactivity in gray matter of the anterior cingulate p>0.05. **(c)** Representative photomicrographs of HO-1 (green) in close association with a Lewy body (red) with DAPI nuclear counterstain. (d) Representative photomicrographs of HO-1 in cells with and without Lew bodies. **(e)** Quantification of HO-1 in PD samples in cells with and without Lewy bodies p=0.0002 N=159